Available online at www.sciencedirect.com
ScienceDirect
Chinese Journal of Aeronautics 23(2010) 39-45
Chinese Journal of Aeronautics
www.elsevier.com/locate/cja

Experimental Investigation into Characteristics of Plasma Aerodynamic Actuation Generated by Dielectric Barrier Discharge

Wu Yun[a,b,*], Li Yinghong[b], Jia Min[b], Song Huimin[b], Su Changbing[b], Pu Yikang[a]

[a]*Department of Engineering Physics, Tsinghua University, Beijing 100084, China*

[b]*Engineering College, Air Force Engineering University, Xi'an 710038, China*

Received 2 March 2009; accepted 26 October 2009

Abstract

This article carries out synthetic measurements and analysis of the characteristics of the asymmetric surface dielectric barrier discharge plasma aerodynamic actuation. The rotational and vibrational temperatures of an $N_2(C^3\Pi_u)$ molecule are measured in terms of the optical emission spectra from the N_2 second positive system. A simplified collision-radiation model for $N_2(C)$ and $N_2^+(B)$ is established on the basis of the ratio of emission intensity at 391.4 nm to that at 380.5 nm and the ratio of emission intensity at 371.1 nm to that at 380.5 nm for calculating temporal and spatial averaged electron temperatures and densities. Under one atmosphere pressure, the electron temperature and density are on the order of 1.6 eV and 10^{11} cm^{-3} respectively. The body force induced by the plasma aerodynamic actuation is on the order of tens of mN while the induced flow velocity is around 1.3 m/s. Starting vortex is firstly induced by the actuation; then it develops into a near-wall jet, about 70 mm downstream of the actuator. Unsteady plasma aerodynamic actuation might stimulate more vortexes in the flow field. The induced flow direction by nanosecond discharge plasma aerodynamic actuation is not parallel, but vertical to the dielectric layer surface.

Keywords: plasma aerodynamic actuation; dielectric barrier discharge; optical emission spectroscopy; particle image velocimetry

1. Introduction

Developed on the basis of the plasma aerodynamic actuation, the plasma flow control is a novel active technique to improve aircraft aerodynamic characteristics and propulsion efficiency[1]. It has drawn considerable attention and found wider and wider applications in boundary layer acceleration[2], airfoil separation control[3-6], forebody separation control[7], turbine blade separation control[8], axial compressor stability extension[9], heat transfer[10] and high-speed jet control[11]. The plasma aerodynamic actuators have a number of merits, such as robustness, simplicity, low power consumption and ability in real-time control at high frequencies.

In order to better understand the underlying physical mechanism of plasma flow control and optimize the geometric configuration of the actuator, it is essential to investigate the characteristics of the plasma aerodynamic actuation including gas temperature, electron density and temperature, induced body force, velocity and vorticity. J. R. Roth[12] measured and analyzed the aerodynamic flow acceleration through paraelectric and peristaltic electrohydrodynamic effects. C. L. Enloe, et al.[13]obtained the emission characteristics of a surface dielectric barrier discharge plasma by means of a photomultiplier and measured the induced thrust with a mass balance. J. Pons, et al.[14] investigated electric properties and induced airflow characteristics of an asymmetric surface barrier discharge plasma aerodynamic actuator by using electric probes and a Pitot tube. T. N. Jukes, et al.[15]studied the velocity and temperature distribution around the plasma aerodynamic actuator by using a hot-wire and cold-wire anemometry. C. O. Por-

*Corresponding author. Tel.: +86-29-84787527-608.
E-mail address: wuyun1223@126.com
Foundation items: National Natural Science Foundation of China (50906100); China Postdoctoral Science Foundation(20090450373)

 doi:10.1016/S1000-9361(09) 60185-01

ter, et al.[16]conducted temporal and averaged body force measurements with a momentum balance, a pendulum and an accelerometer. T. Abe, et al.[17]elucidated the effects of ambient-gas pressure, ambient gas species and electrode configuration through investigation of the momentum transfer in a dielectric barrier discharge plasma aerodynamic actuator. C. A. Borghi, et al.[18] measured the boundary layer, plasma sheath, rotational and vibrational temperatures making use of a Pitot probe, Schlieren imaging and spectroscopic techniques. S. A. Stanfield, et al.[19] examined vibrational temperatures and relative concentrations of $N_2(C^3\Pi_u)$ and $N_2^+(B_2\Sigma_u)$ for an asymmetric surface dielectric barrier discharge utilizing the optical emission spectroscopic technique. C.Q.Nie, et al.[20] investigated the characteristics of the flow induced by the plasma aerodynamic actuation with particle image velocimeter and laser doppler velocimeter. Y. H. Li, et al. [21] investigated the optical emission spectroscopy of a surface dielectric barrier discharge plasma aerodynamic actuator by varying electrode configuration, applied voltage and driving frequency. Y. Wu, et al. [22] studied the electrical, optical, and mechanical characteristics of surface dielectric barrier discharge plasma aerodynamic actuation at different operating pressures ranging from 2 Torr to 760 Torr(1 Torr=133.3 Pa).

This article is aimed at experimentally exploring the characteristics of the asymmetric surface dielectric barrier discharge plasma aerodynamic actuation, which include rotational and vibrational temperatures, electron density and temperature, induced body force, velocity and vorticity.

2. Experimental

2.1. Plasma aerodynamic actuator

Fig.1 shows the schematic diagram of an asymmetric surface dielectric barrier discharge plasma aerodynamic actuator. The dielectric layer used is a plate RO4350B from Rogers Corporation with a relative permittivity of 3.48. The electrodes are made of copper lagged with a lead-tin film. In Fig.1, d_1=2 mm, d_2=2 mm, Δd=0 mm, h_d=0.5 mm, h_e= 0.035 mm.

The plasma aerodynamic actuator is driven by a high-frequency high-voltage power supply CTP-2000K from Suman electronics. The output voltage ranges from 0 to 40 kV and the frequency from 6 kHz to 40 kHz.

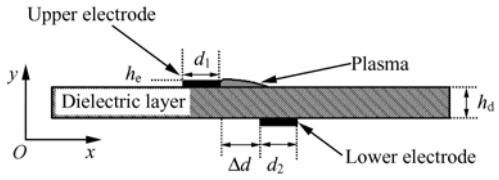

Fig.1 A schematic of an asymmetric surface dielectric barrier discharge plasma aerodynamic actuator.

2.2. Diagnostics system

Fig.2 shows the experimental arrangement. Both the plasma and the induced flow characteristics of the plasma aerodynamic actuation are measured synthetically.

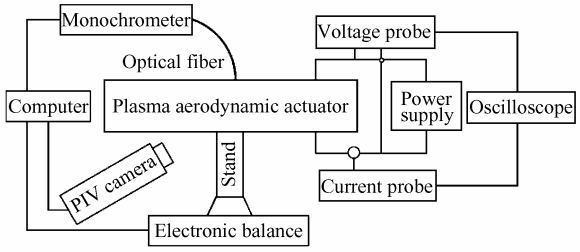

Fig.2 Schematic diagram of experimental arrangement.

A high voltage probe P6015A and a current probe TCP312+TCPA300 from Tektronix Inc. are used to measure the applied voltage and the total discharge current respectively. Signals are recorded by an oscilloscope DPO4104 from Tektronix Inc. Optical emission spectroscopy (OES) is fomulated with a 0. 5 m monochrometer TRIAX550 from Jobin Yvon Inc. through an optical fiber collector located 1 cm over the surface of the dielectric layer. The detector of the monochrometer is a set of photon counting system Model 76915 from Oriel Inc. with a slit width of 20 μm and a calibrated resolution of 0.05 nm. The emission intensity is averaged on time domain and space domain. The body force induced by the plasma aerodynamic actuation is measured with an electronic balance ABS 204-S from Mettler Toledo Inc. Velocity and vorticity induced by the plasma aerodynamic actuation is measured with a particle image velocimeter from Lavision. The air is seeded by vaporization of mineral oil with a mean size of about 0. 3 μm.

3. Results and Discussion

With an enough large alternating current (AC) amplitude on the electrodes, the air is weakly ionized in the region with the largest electric potential. Coulomb force acting on the charged species in the plasma causes momentum transfer between ions and neutral molecules. An air flow is stimulated by the body force. The characteristics of both the plasma

and the induced flow are measured and analyzed.

3.1. Characteristics of plasma

As a simple and non-intrusive diagnostic method, the OES assumes a key role in providing qualitative and quantitative information about plasma properties under atmospheric pressure. Several plasma parameters inclusive of gas temperature, vibrational temperature, electron temperature and density can be successfully identified with the OES method in this study.

The major spectra come from the second positive system (SPS) of $N_2(C^3\Pi_u \rightarrow B^3\Pi_g)$, and the first negative system(FNS) of N_2^+ $(B^2\Sigma_u^+ \rightarrow X^2\Sigma_g^+)$[21] with the relative concentration of $N_2(C^3\Pi_u)$ much greater than that of $N_2^+(B^2\Sigma_u^+)$. The emitting species of $N_2(C^3\Pi_u)$ and N_2^+ $(B^2\Sigma_u^+)$ mainly come from the following excitation processes out of the ground state of N_2 [23].

$$e + N_2(X) \rightarrow e + N_2(C) \quad (E_{th}=11\ \text{eV}) \tag{1}$$

$$e + N_2(X) \rightarrow e + e + N_2^+(B) \quad (E_{th} = 19\ \text{eV}) \tag{2}$$

where e is electron, E_{th} the transition energy, 1 eV=11605 K.

Other main dynamic/kinetic processes in this surface discharge include[24-28]

$$e + N_2(X,\nu) \rightarrow e + N_2(X,\omega) \tag{3}$$

$$N_2(X,\nu) + N_2(X,\omega) \rightarrow N_2(X,\nu-1) + N_2(X,\omega+1) \tag{4}$$

$$N_2(X,\nu) + N_2 \rightarrow N_2(X,\nu-1) + N_2 \tag{5}$$

$$N_2(C) + N_2, O_2 \rightarrow N_2, O_2 + \text{product} \tag{6}$$

$$N_2(C) \rightarrow N_2(B) + h\nu \tag{7}$$

$$N_2^+(B) + N_2, O_2 \rightarrow N_2, O_2 + \text{product} \tag{8}$$

$$N_2^+(B) \rightarrow N_2^+(X) + h\nu \tag{9}$$

where ν and ω are the vibrational quantum numbers, h is the Planck constant.

With the amplitude of applied voltage rising, the emission intensity increases thanks to the electric field strength augmenting. So does it with the driving frequency going up.

Fig.3 illustrates the emission intensity that varies at 337.1 nm in the x direction. The voltage waveform is sinusoidal. The applied voltage is 10 kV (peak to peak) and the driving frequency 23 kHz. A maximum can be observed in the vicinity of the upper electrode where the strength of electric field is the largest.

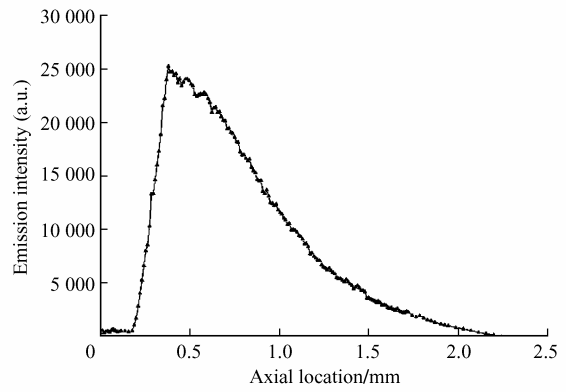

Fig.3 Variation of emission intensity at 337.1 nm in x direction.

During atmospheric discharge, the gas temperature can be estimated with the rotational temperature of a molecular because the rotational energy levels are closely spaced (10^{-3} eV) and allow for rapid energy transfer between the two energy modes[29]. The population distribution at the rotational energy level of N_2 is also believed to comply with Boltzmann distribution due to dense collision between molecules. Here, the rotational temperature of N_2 is acquired through fitting the N_2 second positive system band from 378 nm to 381 nm for the 380.5 nm (ν'=0, ν''=2) N_2 line[30]. By assuming a rotational temperature and taking into account the dipole radiation probability and the response function of the monochrometer, the profile of a certain emission band can be calculated. Thus the actual rotational temperature(T_r) can be determined by comparing the experimentally measured data to the theoretically calculated data.

In the present atmospheric surface discharge, the vibrational excitation of nitrogen seems to be of the utmost importance. $N_2(C^3\Pi_u)$, which is not in a metastable state, generates out of the ground-state electron impact excitation and the cascading effect is not important for the $N_2(C^3\Pi_u)$ state population. Therefore, the vibrational temperature can be determined according to the ratio of two lines in the $N_2(C)$ second positive system[31]. The spectra lines at 371.1 nm and 380.5 nm are selected to be the base for calculating the vibrational temperature (T_v) as follows:

$$\frac{I_{371.1\text{nm}}}{I_{380.5\text{nm}}} = 1.138\,4\exp(-0.495\,2/T_v) \tag{10}$$

Given the amplitude of applied voltage equal to 10 kV(peak to peak) and the driving frequency 23 kHz, the rotational and vibrational temperatures of $N_2(C^3\Pi_u)$ are 0.043 eV and 0.22 eV respectively. The rotational temperature is insensitive to the applied voltage and the driving frequency[21] so is the vibrational temperature (see Fig.4) .

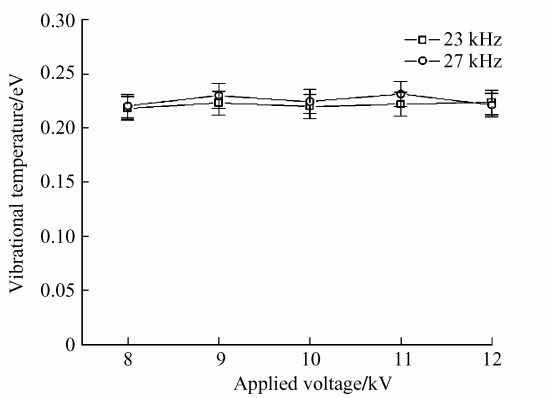

Fig.4 Vibrational temperature vs applied voltage at different driving frequencies.

The zero-dimensional rate balance equation in terms of the concentration, n_v, of molecules (where v means the vth vibrational level of the ground state) is

$$\frac{\mathrm{d}n_v}{\mathrm{d}t} = n_e \sum_{\omega \neq v} n_\omega C_\omega^v - n_e n_v \sum_{\omega \neq v} C_v^\omega + n_{v-1} \cdot \sum_\omega n_{\omega+1} Q_{v,v-1}^{\omega+1,\omega} + n_{v+1} \sum_\omega n_\omega Q_{v+1,v}^{\omega,\omega+1} - n_v \left(\sum_\omega n_{\omega+1} Q_{v,v+1}^{\omega+1,\omega} + \sum_\omega n_\omega Q_{v,v-1}^{\omega,\omega+1} \right) + n_{v+1} \sum_\omega n_\omega Q_{v+1}^v - n_v \sum_\omega n_\omega Q_v^{v-1} \quad (11)$$

where Q and C are rate coefficients of collision.

The rate balance equation for each excited state is:

For state $N_2(C)$,

$$\frac{\mathrm{d}n_\mathrm{C}}{\mathrm{d}t} = n_\mathrm{e} n_{\mathrm{N}_2} Q_\mathrm{C} - A_\mathrm{C} n_\mathrm{C} - n_\mathrm{C} n_{\mathrm{N}_2} Q_{\mathrm{N}_2} - n_\mathrm{C} n_{\mathrm{O}_2} Q_{\mathrm{O}_2} \quad (12)$$

For state $N_2^+(B)$,

$$\frac{\mathrm{d}n_{\mathrm{B}+}}{\mathrm{d}t} = n_\mathrm{e} n_{\mathrm{N}_2} Q_{\mathrm{B}+} - A_{\mathrm{B}+} n_{\mathrm{B}+} - n_{\mathrm{B}+} n_{\mathrm{N}_2} Q_{\mathrm{N}_2} - n_{\mathrm{B}+} n_{\mathrm{O}_2} Q_{\mathrm{O}_2} \quad (13)$$

where A is the Einstein coefficient.

The intensity ratio of optical emission line from FNS to SPS strongly depends on the electron temperature or the energy distribution function for the electrons with the energy more than 11 eV because the excited thresholds of the two processes have a difference of about 8 eV[23]. According to Eq. (12) and Eq. (13) , the electron temperature (T_e) can be calculated using the intensity ratio of 391.4 nm and 380.5 nm:

$$\frac{I_{391.4nm}}{I_{380.5nm}} = K_0 \cdot (T_e)^{C_0} \cdot \exp(-\frac{E_0}{T_e}) \quad (14)$$

where K_0, C_0 and E_0 are constants by fitting experimental data.

Eq.(12) and Eq.(13) evince that the relative intensity of different vibrational levels of $N_2(X)$ is mainly determined by the electron density. According to the Frank-Condon principle, the distribution of vibrational energy level of $N_2(C)$ can be found by using the changes in that of $N_2(X)$. Therefore, the ionization rate n can be calculated through the ratio of the intensity at 371.1 nm to that at 380.5 nm:

$$\frac{I_{371.1\mathrm{nm}}}{I_{380.5\mathrm{nm}}} = C_0 + C_1 \lg(n) + C_2 (\lg n)^2 \quad (15)$$

The electron temperature is 1.63 eV and the electron density is 1.1×10^{11} cm^{-3} under the applied voltage of 10 kV. The driving frequency is 23 kHz. Under one atmospheric pressure, the electron temperature is usually 1-2 eV because of frequent collision between electrons and molecules.

The variation of average electron temperature and density with the applied voltage is shown in Fig.5, which displays a slight dependence of the former two upon the latter with its frequency. The electron temperature of a dielectric barrier discharge is strongly affected by the gas pressure because the collision-free path of the electrons mainly determines the energy obtainable by the electrons in the electric field. The frequent collision between electrons and molecules governs the discharge process under one atmosphere pressure.

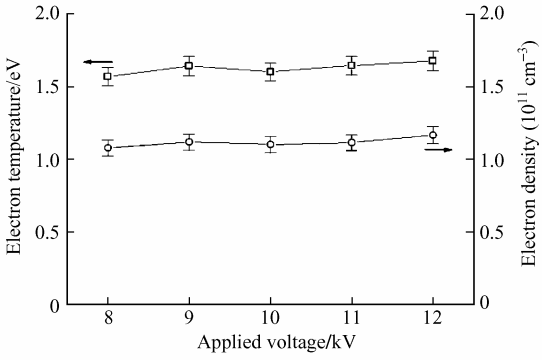

Fig.5 Electron temperature and density vs applied voltage.

3. 2. *Characteristics of induced flow*

Fig.6 shows the induced body force in x direction vs the applied voltage with the driving frequency of 23 kHz. From Fig.6, it can be seen that the body force increases from 11 mN to 65 mN, when the applied voltage rises from 8 kV to 12 kV.

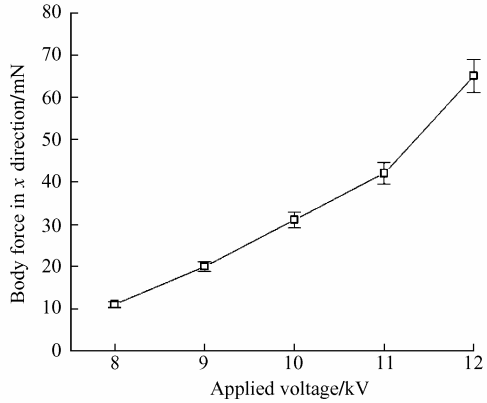

Fig.6 Body force in x direction induced by plasma aerodynamic actuation.

Fig.7(a) shows the starting vortex induced by the steady plasma aerodynamic actuation in static air and Fig.7 (b) the equally induced directed wall jet. The starting vortex exists for about 1 s only and then changes into the directed wall jet about 70 mm downstream of the upper electrode. The induced flow velocity is 1.3 m/s at the applied voltage of 10 kV and the driving frequency of 23 kHz.

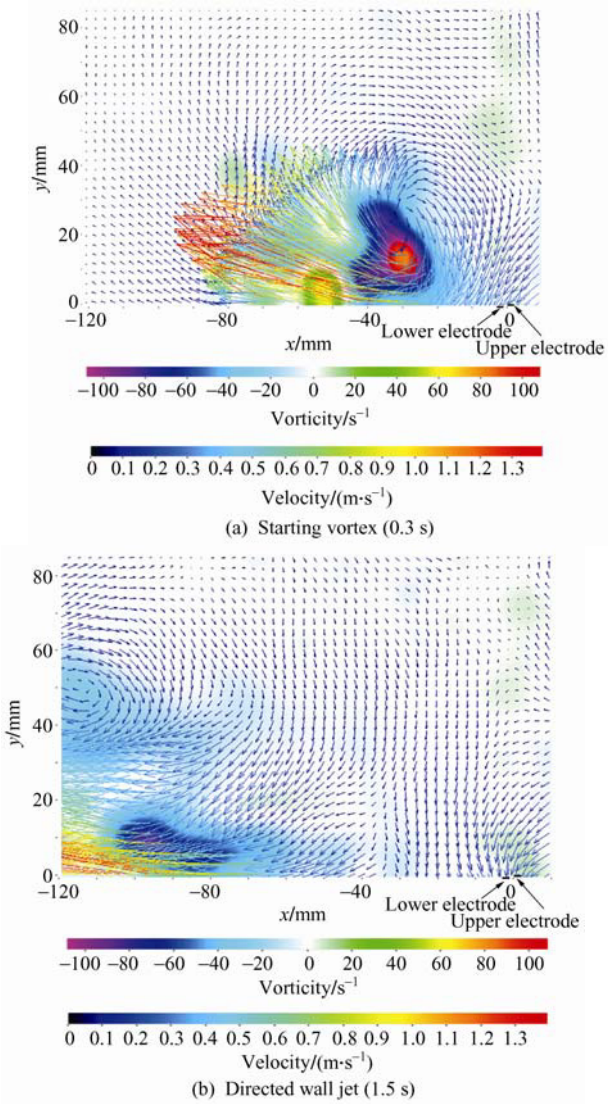

Fig.7 Velocity and vorticity of starting vortex and directed wall jet induced by steady plasma aerodynamic actuation.

When the unsteady plasma aerodynamic actuation begins, the starting vortex seems stronger and lives longer for about 2 s; then it turns into a directed wall jet involving lots of tiny vortexes, about 50 mm downstream of the upper electrode (see Fig.8). This takes place in a stretch amounting to 70% of the cycle time and at an excitation frequency 190 Hz. The unsteady plasma aerodynamic actuation induces much more vortexes in the flow field.

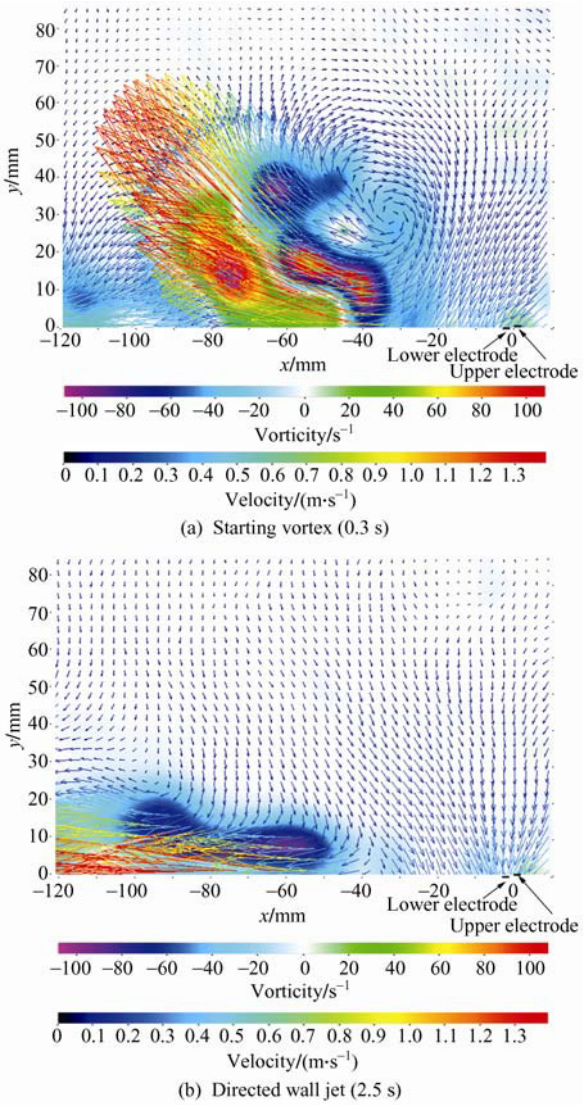

Fig.8 Velocity and vorticity of starting vortex and directed wall jet induced by unsteady plasma aerodynamic actuation.

When the voltage waveform is a nanosecond pulse, not the sinusoidal pulse, the induced flow direction changes remarkably. The induced flow direction by

nanosecond discharge plasma aerodynamic actuation is not parallel, but vertical to the dielectric layer surface (see Fig.9). The voltage pulse has a full wave at half maximum (FWHM) of 190 ns and a rise time of 450 ns. The peak voltage and frequency are 10 kV and 1 kHz, respectively.

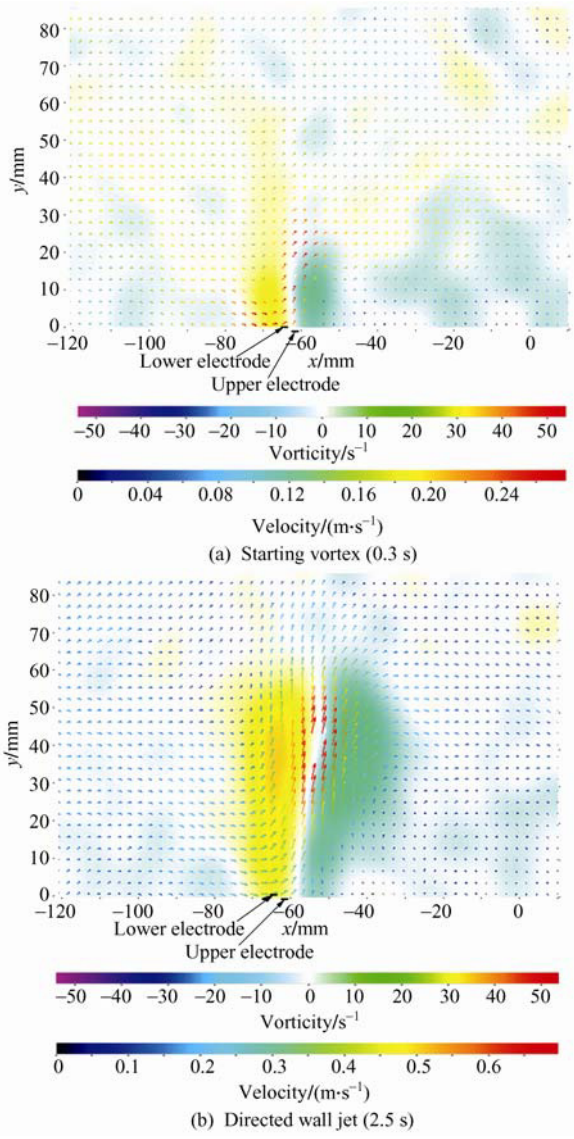

Fig.9 Velocity and vorticity of starting vortex and directed jet induced by nanosecond discharge plasma aerodynamic actuation.

4. Conclusions

In conclusion, the characteristics of both plasma and induced flow of the asymmetric surface dielectric barrier discharge plasma aerodynamic actuation has been experimentally investigated by optical emission spectroscopy diagnosis and measuring body force, velocity and vorticity.

The rotational temperature is around 0.043 eV and the vibrational temperature 0.22 eV while the electron temperature is about 1.6 eV and the electron density 1.1×10^{11} cm^{-3}. The applied voltage and the driving frequency do exert little effect on the vibrational temperature, electron temperature and density. The body force induced by the plasma aerodynamic actuation is on the order of tens of mN. Starting vortexes do form once the actuation begins and then develop into a near-wall jet, about 70 mm downstream of the actuator. The unsteady actuation induces much more vortexes in the flow field. The induced flow direction by nanosecond discharge plasma aerodynamic actuation is vertical to the dielectric layer surface.

Acknowledgement

The authors would like to thank Guo Zhigang, Zhu Ximin, Hu Dawei and Chen Wencong for their valuable help in the experiments.

References

[1] Corke T C, Post M L, Orlov D M. Single-dielectric barrier discharge plasma enhanced aerodynamics:concepts, optimization, and applications. Journal of Propulsion and Power 2008; 24(5):935-945.

[2] Roth J R, Sherman D M. Electrohydrodynamic flow control with a glow-discharge surface plasma. AIAA Journal 2000; 38(7):1166-1172.

[3] Roupassov D V, Nikipelov A A, Nudnova M M, et al. Flow separation control by plasma actuator with nanosecond pulsed-periodic discharge. AIAA Journal 2009; 47(1):168-185.

[4] Mao M L, Deng X G, Chen J Q. Numerical simulation of flow control past a stalled airfoil with OAUGDP. Acta Aerodynamica Sinica, 2008; 26(3): 334-338. [in Chinese]

[5] Zhang P F, Wang J J, Shi W Y, et al. Experimental study on the separation control by plasma actuator in subsonic flow. Journal of Experiments in Fluid Mechanics 2007; 21(2):35-39. [in Chinese]

[6] Li Y H, Liang H, Ma Q Y, et al. Experimental investigation on airfoil suction side flow separation suppression by pulse plasma aerodynamic actuation. Acta Aeronautica et Astronautica Sinica 2008; 29(6): 1429-1435. [in Chinese]

[7] Liu F, Luo S, Gao C, et al. Flow control over a conical forebody using duty-cycled plasma actuators. AIAA Journal 2008; 46(11):2969-2973.

[8] Huang J, Corke T C, Thomas F O. Unsteady plasma actuators for separation control of low-pressure turbine blades. AIAA Journal 2006; 44(7):1477-1487.

[9] Wu Y, Li Y H, Zhu J Q, et al. Experimental investigation of a subsonic compressor with plasma actuation treated casing. AIAA-2007-3849, 2007.

[10] Jayaraman B, Thakur S, Shyy W. Modeling of fluid dynamics and heat transfer induced by dielectric barrier plasma actuator. ASME Journal of Heat Transfer 2007; 129(2):517-525.

[11] Samimy M, Kim J, Kastner J, et al. Active control of high-speed and high Reynolds number jets using plasma actuators. Journal of Fluid Mechanics 2007; 578:305-330.
[12] Roth J R. Aerodynamic flow acceleration using paraelectric and peristaltic electrohydrodynamic effects of one atmosphere uniform glow discharge plasma. Physics of Plasmas 2003; 10(5):2117-2126.
[13] Enloe C L, McLaughlin T E, van Dyken R D, et al. Mechanisms and responses of a single dielectric barrier plasma actuator:plasma morphology. AIAA Journal 2004; 42(3):589-594.
[14] Pons J, Moreau E, Touchard G. Asymmetric surface dielectrical barrier discharge in air at atmospheric pressure:electrical properties and induced airflow characteristics. Journal of Physics D:Applied Physics 2005; 38(19):3635-3642.
[15] Jukes T N, Choi K, Johnson G A, et al. Characterization of surface plasma-induced wall flows through velocity and temperature measurements. AIAA Journal 2006; 44(4):764-771.
[16] Porter C O, Baughn J W, McLaughlin T E, et al. Plasma actuator force measurements. AIAA Journal 2007; 45(7):1562-1570.
[17] Abe T, Takizawa Y, Sato S, et al. Experimental study for momentum transfer in a dielectrical barrier discharge plasma actuator. AIAA Journal 2008; 46(9):2248-2256.
[18] Borghi C A, Carraro M R, Cristofolini A, et al. Electrohydrodynamic interaction induced by a dielectric barrier discharge. Journal of Applied Physics 2008; 103(6):063304.
[19] Stanfield S A, Menart J. Vibrational temperatures and relative concentrations of $N_2(C_3\Pi_u)$ and $N_2^+(B_2\Sigma_u)$ for an asymmetric surface mode dielectric barrier discharge. AIAA-2009-0653, 2009.
[20] Nie C Q, Li G, Zhu J Q, et al. Investigation of dielectric barrier discharge plasma flow control. Science in China Series E: Technological Sciences 2008; 51(7); 1064-1072.
[21] Li Y H, Wu Y, Jia M, et al. Optical emission spectroscopy investigation of a surface dielectric barrier discharge plasma aerodynamic actuator. Chinese Physics Letters 2008; 28(11):4068-4071.
[22] Wu Y, Li Y H, Jia M, et al. Influence of operating pressure on surface dielectric barrier discharge plasma aerodynamic actuation characteristics. Applied Physics Letters 2008; 93(3):031503.
[23] Choi J H, Lee T I, Han I, et al. Investigation of the transition between glow and streamer discharges in atmospheric air. Plasma Sources Sciences and Technology 2006; 15(3):416-420.
[24] Zhu X M, Pu Y K. Determining the electron temperature in inductively coupled nitrogen plasmas by optical emission spectroscopy with molecular kinetic effects. Physics of Plasmas 2005; 12(10):103501.
[25] Zhu X M, Pu Y K. A molecular kinetic model for the optical emission spectroscopy technique in inductively coupled nitrogen plasma. Physics of Plasmas 2006; 13(6):063507.
[26] Dilecce G, Ambrico P F, de Benedictis S. OODR-LIF direct measurement of $N_2(C_3\Pi,v=0\text{-}4)$electronic quenching and vibrational relaxation rate coefficients by N_2 collision. Chemical Physics Letters 2006; 431(4-6):241-246.
[27] Dilecce G, Ambrico P F, de Benedictis S. New $N_2(C_3\Pi_u, v)$ collision quenching and vibrational relaxation rate constants:2. PG emission diagnostics of high-pressure discharges. Plasma Sources Science Technology 2007; 16(1):S45-S51.
[28] Kozlov K V, Wagner H E. Progress in spectroscopic diagnostics of barrier discharges. Contribution to Plasma Physics 2007; 47(1-2):26-33.
[29] Ramsay D A. Spectroscopy. London:University Park Press, 1972.
[30] Huang X J, Xin Y, Yang L, et al. Spectroscopic study on rotational and vibrational temperature of N_2 and N_2^+ in dual-frequency capacitively coupled plasma. Physics of Plasmas 2008; 15(11):113504.
[31] Kang Z D, Pu Y K. Molecular nitrogen vibrational temperature in an inductively coupled plasma. Chinese Physics Letters 2002; 19(2):211-213.

Biography:

Wu Yun Born in 1983, he received B.S. and Ph.D. degrees from Air Force Engineering University in 2003 and 2008 respectively, and then became a teacher there. He is now a post-doctorate in Department of Engineering Physics, Tsinghua University. His main research interest is plasma flow control.
E-mail: wuyun1223@126.com